TOPOLOGY AND NON-LINEAR MATCHING: FROM KAM TORI TO BEAM PROFILES

G. Sterbini*, H. Bartosik, A. Fornara, M. Giovannozzi, CERN, Geneva, Switzerland
P. Bélanger, University of British Columbia and TRIUMF, Vancouver, British Columbia

Abstract

In modern circular accelerators, beam mismatch at injection into non-linear lattices can play a crucial role for beam quality degradation. In this work, we explore the process of non-linear matching in the Kolmogorov–Arnold–Moser (KAM) quasi-periodic regime, focusing on how the intrinsic phase-space structure influences the evolution of initial beam distributions. Using a topological approach, we quantify how Gaussian beams can develop non-Gaussian tails when propagated through non-linear focusing elements, as a consequence of the shape of the underlying invariant tori. These results are relevant for the design and operation of high-intensity storage rings and colliders where beam-halo control is critical.

INTRODUCTION

During the injection process between a transfer line and a synchrotron, the problem of beam filamentation and its related beam "emittance dilution" has been systematically studied in the linear approximation (e.g., Refs. [1, 2]).

The aim of this paper is to generalise the problem to the non-linear case. Namely, given

1. a non-linear lattice where we neglect all collective effects (single particle dynamics) and
2. the distribution $f_0(\vec{x},\vec{p})$ at turn $N = 0$ and position s_0,

we aim to find the equilibrium distribution for $N \to \infty$, $f_\infty(\vec{x},\vec{p})$, also referred to as the matched distribution.

Using the progress of modern computing power and tracking codes (see, e.g. Ref. [3]), this problem can be directly addressed, in its most general form, via numerical tracking, e.g. by computing turn-by-turn $f_N(\vec{x},\vec{p})$ and monitoring its evolution from f_N to f_{N+1}.

In non-linear lattices, given the known mechanism of chaotic trajectories and related diffusion, this convergence is ill-posed in a strict mathematical sense. However, in most practical cases, the profile of a mismatched beam converges to a steady state in a fraction of a second.

This is possible because the time constant of the filamentation process, $\tau_{\mathscr{F}}$, is much shorter than that of the diffusive process, $\tau_{\mathscr{D}}$ ($\tau_{\mathscr{F}} \ll \tau_{\mathscr{D}}$). In addition, the extent of possible chaotic layers in quasi-integrable Hamiltonian systems can be neglected for our purpose. In the CERN Large Hadron Collider (LHC), the filamentation process takes a few hundred turns [4], while the diffusive processes (mainly driven by collective effects such as IBS, space charge, electron-cloud, beam-beam, …) have time constants of tens of minutes (see, e.g. Refs. [5–7]).

* guido.sterbini@cern.ch

It is possible to recover the well-posed mathematical meaning of the convergence of f_N to f_{N+1} for $N \to \infty$ by introducing an additional working hypothesis along with the two aforementioned ones, namely $\tau_{\mathscr{D}} \to \infty$. This is equivalent to assuming that all particles of $f_0(\vec{x},\vec{p})$ undergo quasi-periodic motion, i.e., the initial distribution is fully contained in a region where the system is integrable. The existence of such regions follows from the Kolmogorov-Arnold-Moser (KAM) theory, which was developed mainly in the context of the long-term stability of Hamiltonian systems. In fact, it was an essential offspring of perturbation theory, which then enabled important applications to the stability analysis of Hamiltonian systems [8–10]. Here we will focus on its topological implications [11] for the non-linear matching.

In the following, we will comment on the potential and limits of this approach. For clarity, we will remain as close as possible to numerical tracking, maintaining a close connection between simulations, visualisations, and results.

THE 2D HÉNON MAP EXAMPLE

In this section, we show a step-by-step numerical approach, assuming

1. the simplest non-linear map, the 1-degree-of-freedom quadratic Hénon map (see Eq. 5.1.2 of [12])

$$z_{N+1} = e^{i2\pi Q_x}\left[z_N - \frac{i}{4}\left(z_N + z_N^*\right)^2\right], \qquad (1)$$

   where $z_N = x_N - i\,p_{x,N}$ is the phase space position at turn N and Q_x is the map's tune,
2. a uniform beam distribution

$$f_0 = \begin{cases} \dfrac{1}{\pi r^2}, & \text{if } x^2 + p_x^2 < r^2, \\ 0, & \text{otherwise.} \end{cases} \qquad (2)$$

The same approach can be easily applied to different non-linear lattices and distributions. In fact the analysis is performed on the resulting turn-by-turn data and is based on the only assumption of quasi-periodic motion. Without loss of generality, we consider a linearly normalised phase space (thus, the units of x and p_x are expressed in units of $\sqrt{\text{m}}$).

Using the Xsuite tracking code [3], we can compute, for a given set of initial conditions (e.g. linearly distributed in $0 \le x \le 0.5\ \sqrt{\text{m}}$ with $p_x = 0$ and tune $Q = 0.2071$ [12]), their $(x, p_x)|_N$ coordinates for $N_{\max} = 5$ kturns, as in Fig. 1.

If the distribution of Eq. (2) is non-vanishing in the region of resonant stable islands of Fig. 1, the limit distribution $f_\infty(x, p_x)$ will not, in general, converge, i.e., we will observe persisting envelope oscillations in the x-projected profile of f_∞. For simplicity, we will assume that the distribution

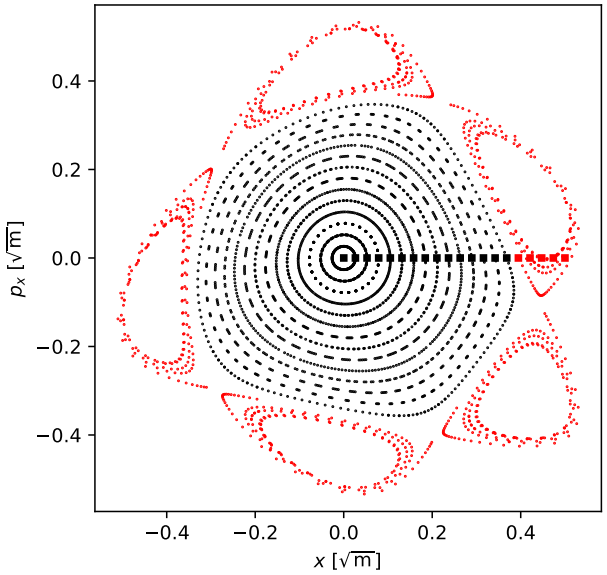

Figure 1: Turn-by-turn phase-space evolution with $0 \leq N < 200$ of 20 particles (initial conditions are marked with squares).

vanishes in the regions of the resonance islands (Fig. 1, in red), e.g. $r \lesssim 0.3\ \sqrt{\text{m}}$ in Eq. (2). We will therefore focus on the tori around the fixed point of periodicity 1 (the origin of the $x - p_x$ plane).

For each of the 15 initial conditions (particles) of Fig. 1, we can associate a torus. To find a numerical expression for this set of tori (a foliation of tori) we

1. compute orbit spectra with the NAFF algorithm [13–15]
2. perform frequency identification (FI) [16], i.e. express each spectral frequency as harmonic combination of the fundamental frequencies (the "tunes").

The aforementioned steps can be performed using the packages `nafflib` [17] and `pytori` [18], respectively. By performing step 1, we assume that the motion of the particle is quasi-periodic (KAM region assumption). Step 2 (sorting) is more complex when we consider 4D or 6D motion [11]. As an example, the harmonic content of particle #15 (Fig. 1) is presented in Fig. 2 (top), truncated to its first 50 harmonics. Particle #15 is the largest-amplitude one, lying on the outermost torus (and that with the richest frequency content, being very close to the inner side of the separatrix around the stable islands). It is clear that the first 5 harmonics are the most excited, indicating proximity to the 5^{th}-order resonance (that of the islands in Fig. 1). Given the nine orders of magnitude between the first and the $h = 26$ harmonic (Fig. 2 (bottom)), the spectrum could be further truncated. The convergence as a function of harmonic content of the torus associated with particle #15 is shown in Fig. 3: the first 10 harmonics are sufficient to represent it within a reasonably small error compared to the scale of the plot's axes. Tori closer to a resonance will require more harmonics to be represented with similar accuracy.

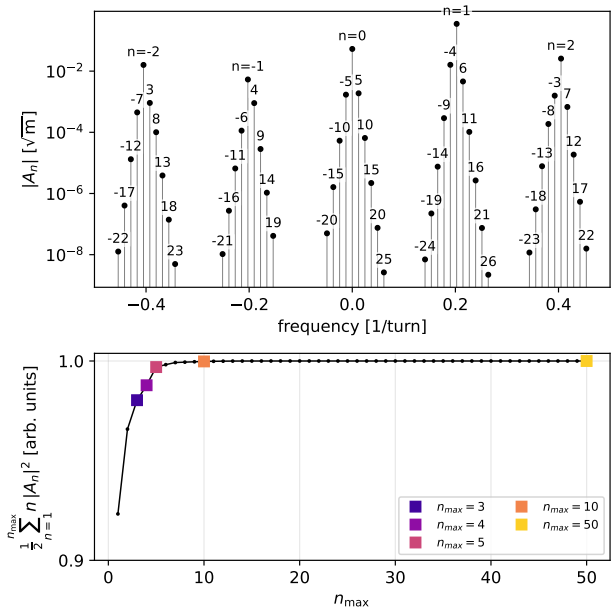

Figure 2: Top: Harmonic content of the spectrum of particle #15. The labels refer to the harmonic of the fundamental frequency (tune). To be noted that the corresponding torus is not centred in $(0, 0)$, therefore the $n = 0$ harmonic is not vanishing. Bottom: Convergence plot of the torus action (see Eq. (5)), normalized to its value at $n_{\max} = 50$.

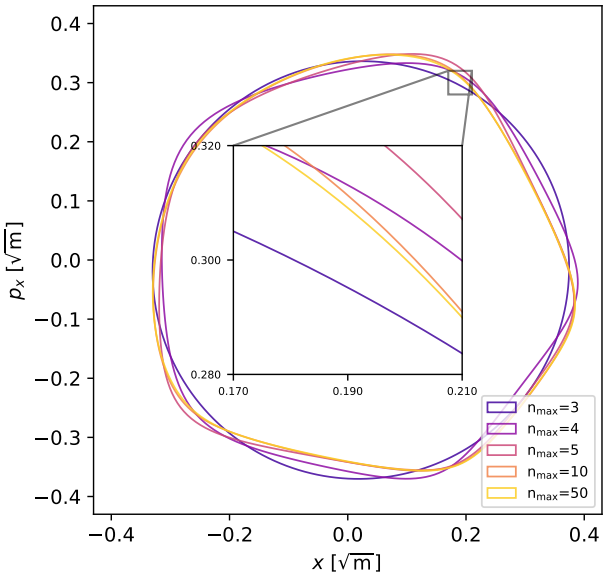

Figure 3: Convergence study versus harmonic content of the torus associated with the orbit of particle #15.

The $x - p_x$ phase-space position of each particle at turn N can be represented by a Fourier expansions expressed in terms of its set of frequencies Q_n

$$x(N) - ip_x(N) = \sum_n A_n e^{i\,2\pi Q_n N} \overset{\text{FI}}{=} \sum_n A_n e^{i\,n\,\overbrace{2\pi Q_x N}^{\theta_x}}, \quad (3)$$

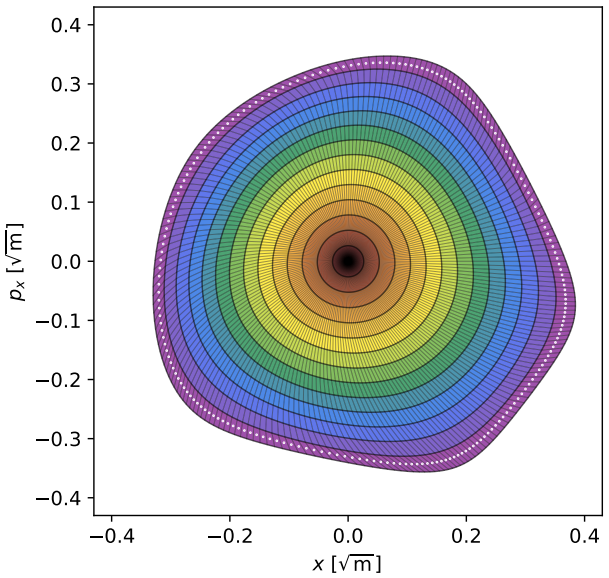

Figure 4: A foliation of the phase space in tori. The different slabs are colour-coded. Each slab is divided into 200 sectors.

and after FI, instead of following the particle at turn N, we can express its associated torus as

$$x(\theta_x) - ip_x(\theta_x) = \sum_n A_n e^{i\,n\theta_x} \tag{4}$$

where $\theta_x \in [0, 2\pi)$ is the angular coordinate along the torus, while the action of the torus, I_x, is the area enclosed by the torus normalised by 2π [19]. One can express the action of the torus as a function of the A_n coefficients of its spectrum (see Eq. (2.28) of [11] for the 6D generalisation):

$$I_x = \frac{1}{2}\sum_n n|A_n|^2. \tag{5}$$

Equation (4) allows us to express the turn-by-turn representation of the 15 particles of Fig. 1 as a foliation of 15 tori (or leaves), as in Fig. 4. The region between two tori is called a slab, and the region of a slab between $\theta_1 \le \theta_x \le \theta_2$ is called a sector. In Fig. 4, each slab is partitioned into 200 sectors with the same extent $\Delta\theta_x = \frac{2\pi}{200}$. In the outermost slab of Fig. 4 we plotted, for each sector, its centre (white dot), i.e. the average of the vertices of the sector.

The infinitesimal area, $d\mathscr{A}$, of each sector (assuming a dense foliation of tori) is

$$d\mathscr{A} = dI_x d\theta_x, \tag{6}$$

where dI_x is the difference between the actions of the two tori that bound the slab. Within an error that can be reduced at will by increasing the density of the foliation, sectors belonging to the same slab have identical area. In fact, there is a symplectic mapping (i.e. that preserves the sector areas) that transports the topology of Fig. 4 to a purely polar topology, which is given by the normal form, where sectors belonging to the same slab clearly have the same area.

We can numerically construct this map by associating to each sector a symplectic matrix

$$M = e^{\Omega\, S_1} e^{\Omega\, S_2}, \tag{7}$$

with $S_{1,2} = S_{1,2}^T$ and $\Omega = \begin{pmatrix} 0 & 1 \\ -1 & 0 \end{pmatrix}$. The matrix M transports a generic sector of Fig. 4 to its corresponding polar sector $(\Delta r_x,\ \Delta\theta_x)$ with $\sqrt{2I_1} < \Delta r_x < \sqrt{2I_2}$ and $\theta_1 < \Delta\theta_x < \theta_2$. For each sector, M is the Jacobian of the normalisation map evaluated in the centre of the sector.

FROM KAM TORI TO BEAM PROFILES

Once we have defined the foliation of KAM tori as described in the previous section, the next natural step is to use it as a mesh to represent the beam distribution. Each sector of the foliation will correspond to a cell of the mesh.

We will assign to the centre of each cell a value $f_{0,\mathrm{c}}$, proportional to the initial beam distribution density, f_0, evaluated at the cell vertices; in other words, we will consider a cell-centred mesh rather than a node-centred one. It is important to note that, in general, cells belonging to different slabs have different areas, which is a natural consequence of the linear spacing of the initial conditions as in Fig. 1. For this reason, it is important to weight the cell-centre value by the cell area

$$f_{0,\mathrm{c}} \propto \mathscr{A}_\mathrm{c} \sum_{v\in\mathscr{V}(\mathrm{c})} f_0(v) \tag{8}$$

where $\mathscr{V}(\mathrm{c})$ denotes the set of cell vertices.

To maintain the condition $\sum_{\mathrm{c}\in\mathrm{cells}} f_{0,\mathrm{c}} = 1$, the expression in Eq. (8) must be appropriately normalised.

In Fig. 5, we used a much denser tori foliation than in the example of Fig. 4, and the $f_{0,\mathrm{c}}$ values corresponding to the density of Eq. (2) (with $r = 0.33$) are shown (colour coded) at the centres of the mesh cells. Although the initial density is uniform, the weighting by cell area yields, as expected, a non-uniform $f_{0,\mathrm{c}}$ (blue tones indicate lower values, close to the origin of phase space, where the cell areas are smaller).

Projecting the meshed distribution onto the x-axis gives, within the numerical accuracy of the finite mesh, the x-profile obtained by the Abel transform, $\propto \max(\sqrt{r^2 - x^2},\ 0)$, of the uniform distribution (see Fig. 6). It is important to note that even if the mesh is not rotationally symmetric, f_0 should be. As an additional sanity check, we can verify that projecting the initial distribution (after rotations of $\pi/4$, $\pi/2$, and $3\pi/4$) gives the same x-profile, within the numerical accuracy of the finite mesh.

To find the matched density representation on our mesh, we simply assign to each slab a slab-averaged value $f_{\mathrm{slab}} = \langle f_{0,\mathrm{c}}\rangle_{\mathrm{slab}}$. In fact, the initial density of the slab will be constrained to filament between the two tori bounding the slab: the natural detuning of the action differential dI_x will act on the initial slab distribution until it becomes θ_x-invariant. The result of this averaging is shown in Fig. 7, while the corresponding x-projections are shown in Fig. 8.

It is important to note that the distributions develop tails as a result of filamentation. Although the rms width of these profiles is larger than that of the initial profile (Fig. 6), by construction, $\langle I_x\rangle$ of the distribution (and, more generally, pdf(I_x)) is an invariant of the filamentation process (symplectic mapping). In fact, while the s-invariant beam profile

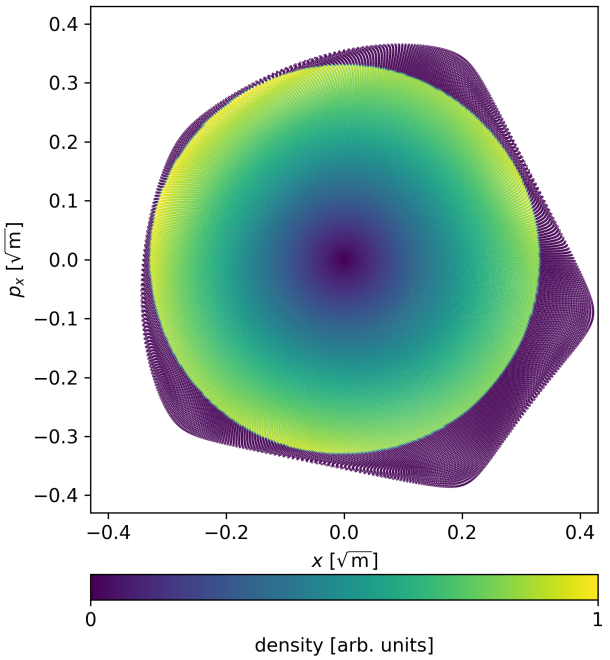

Figure 5: Initial distribution represented on the mesh derived from the tori foliation.

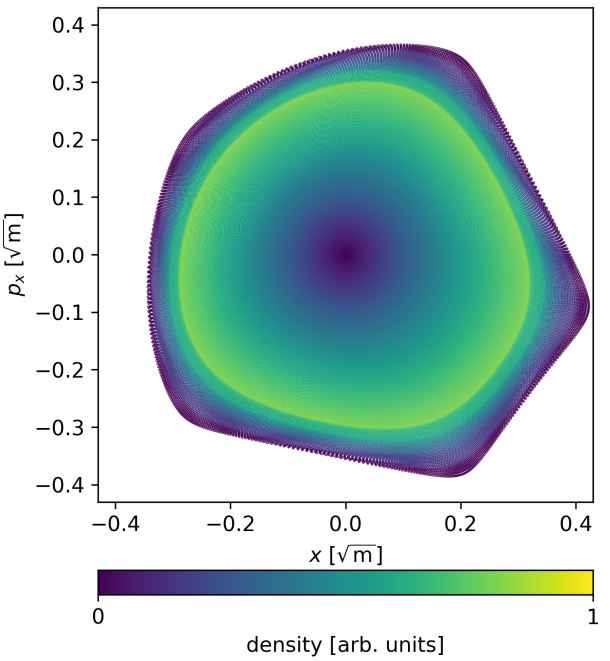

Figure 7: Final distribution represented on the mesh derived from the tori foliation.

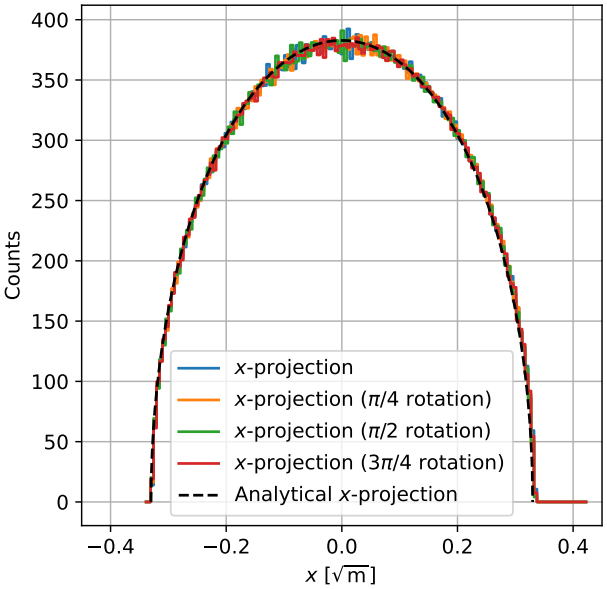

Figure 6: x-projection of the initial distribution.

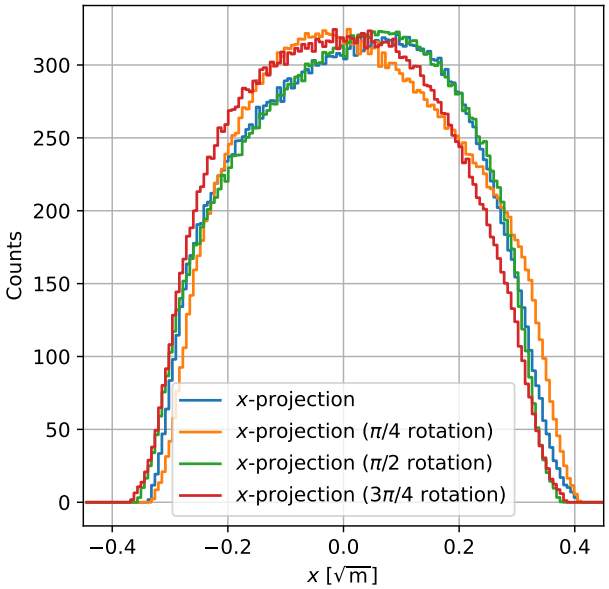

Figure 8: Beam profiles of the matched distribution.

is a well-posed concept for linear lattices (after a suitable x-scaling), in the presence of non-linearities (within our KAM-region approximation), the profiles change along the longitudinal coordinate s: the 4 profiles of Fig. 8 could correspond to different Poincaré sections of the Hamiltonian flow, and only pdf(I_x) is an s-invariant. Furthermore, the x-profile is in general not symmetric with respect to the $x = 0$ axis.

The analysis presented for the distribution of Eq. (2) can be easily repeated for other distributions, for example a 2D Gaussian distribution with $\sigma = 0.055$ truncated at $6\,\sigma$. In Fig. 9, the results for the different x-projections (with the usual rotations) are reported and compared to the x-projections of the initial distribution. It is clearly visible that, for the system and the initial distribution considered, heavier tails develop.

KAM TORI AND GENERALISATION OF THE ABEL TRANSFORM

The Abel transform offers an invaluable tool for reconstructing the transverse beam distribution from transverse beam profiles in linear lattices [20, 21]. A tori foliation, as represented in Fig. 4, also offers a natural way to numerically

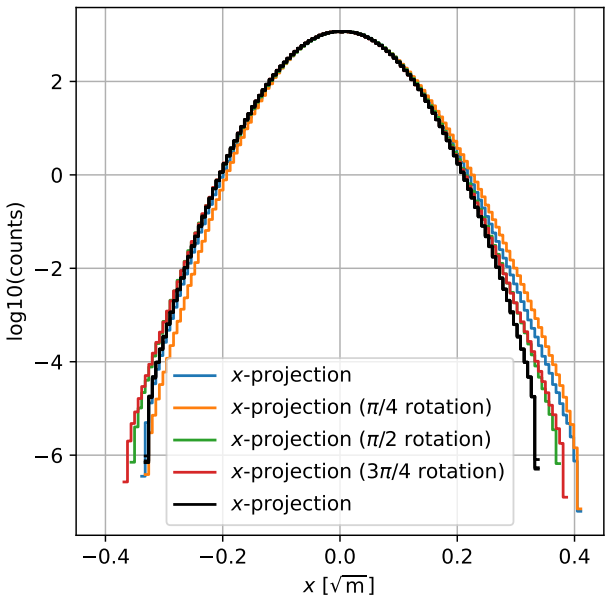

Figure 9: Result of the matching of a truncated Gaussian.

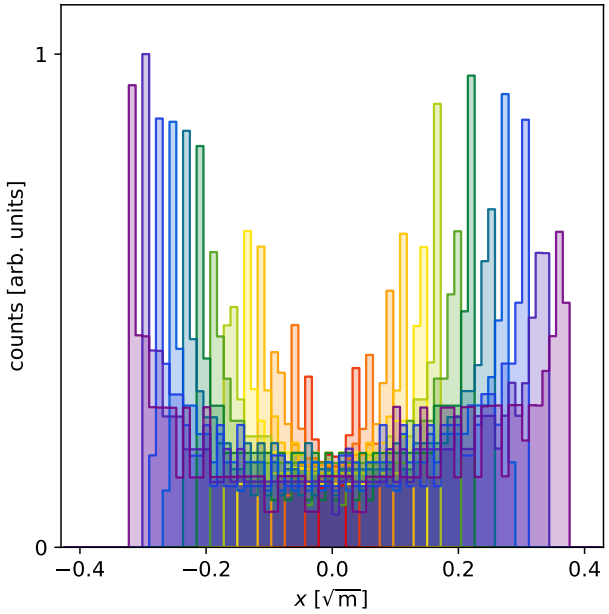

Figure 10: x-projected slabs of the tori foliation of Fig. 4.

reconstruct a matched beam distribution from the x-profiles. We can construct a set of x-profiles corresponding to each slab of the foliation (see Fig. 10), and solve a non-negative least-squares problem (or perform an elimination algorithm starting from the largest-amplitude slab) to find the density of each individual slab. In normal form, the projection of the slabs is proportional to the kernel (x-symmetric) of the Abel transform ($\propto \frac{1}{\sqrt{r^2-x^2}}$ for $x < r$, where r is the radius of the torus). Examining Fig. 10, we can recognise the $\frac{1}{\sqrt{r^2-x^2}}$ symmetric behaviour of the low-amplitude slabs, while the outer slabs are asymmetric with respect to the $x = 0$ axis (as observed in the profiles of Figs. 8 and 9).

CONCLUSIONS

The concept of a "matched distribution" implicitly assumes that the initial beam distribution is fully contained within a pseudo-KAM region, i.e. a region of phase space where particle motion is quasi-periodic and the system is integrable in the KAM sense. This working hypothesis, while not strictly rigorous in the presence of chaotic motion and diffusion, is well justified in practice by the separation of time scales between the filamentation process and the diffusive processes. We have shown that a foliation of KAM tori provides a natural cell-centred mesh to represent the beam distribution and that this framework enables three related applications:

1. the computation of the beam distribution after filamentation, as the slab-averaged density;
2. the computation, for each cell, of the local symplectic matrix and the associated quadratic Hamiltonian;
3. the reconstruction of the matched beam distribution from measured transverse beam profiles, as a generalisation of the Abel transform to non-linear lattices.

We have shown that, although pdf(I_x) is an invariant of the filamentation process, the transverse beam profile is not: it changes along the longitudinal coordinate s and, in general, is not symmetric with respect to the $x = 0$ axis. This has direct practical implications for the characterisation of beam quality at injection: quantities such as the variance or the parameters of a q-Gaussian fit to the beam profile are not, in general, s-invariant in the presence of non-linearities. Consequently, the q-Gaussian parameters describing the beam profile at injection can be affected by non-linear elements such as strong octupoles, high chromaticity settings, or beam–beam interactions. As the LHC, and in particular the High-Luminosity LHC (HL-LHC), operates with increasingly stronger non-linear elements, these effects are expected to become progressively more significant and should be accounted for in beam quality and collimation studies.

The approach presented here, based on the `nafflib` and `pytori` packages and the Xsuite tracking code, is general and can be readily extended to 4D and 6D phase space, paving the way for a systematic non-linear matching framework applicable to the full complexity of realistic accelerator lattices. In addition, a first-order Resonance Driving Terms analysis could offer an alternative to tracking for reconstructing an approximation of the tori foliation.

The authors would like to thank F. Capuani, L. Deniau, I. Efthymiopoulos, B. J. A. Faber, D. Kaltchev, S. Kostoglou, G. Iadarola, E. Lamb, N. Mounet, Y. Papaphilippou, S. Redaelli, R. Tómas, G. Trad, and D. Veres for their valuable discussions and contributions.

REFERENCES

[1] D. Möhl, "Sources of emittance growth", 2006. doi:10.5170/CERN-2006-002.245

[2] G. Arduini and P. Raimondi, "Transverse emittance blow-up due to injection errors", Geneva, 1999, https://cds.cern.ch/record/702522,

[3] G. Iadarola *et al.*, "Xsuite: An Integrated Beam Physics Simulation Framework", in *Proc. HB'23*, Geneva, Switzerland, pp. 73–80, Mar. 2024. doi:10.18429/JACoW-HB2023-TUA2I1

[4] S. Burger *et al.*, "Turn by Turn Profile Monitors for the CERN SPS and LHC", 2013. https://cds.cern.ch/record/1637773

[5] S. Papadopoulou *et al.*, "Monitoring and modelling of the LHC emittance and luminosity evolution in 2018", WEPTS046, 2019. doi:10.18429/JACoW-IPAC2019-WEPTS046

[6] M. Hostettler *et al.*, "Emittance Evolution in the LHC: From Injection to Collisions", pp. 157–160, 2019. https://cds.cern.ch/record/2813547

[7] K. Paraschou *et al.*, "Emittance Growth From Electron Clouds Forming in the LHC Arc Quadrupoles", in *Proc. HB'23*, Geneva, Switzerland, pp. 487–490, Mar. 2024. doi:10.18429/JACoW-HB2023-THBP16

[8] N. Nekhoroshev, "An exponential estimate of the time of stability of nearly-integrable Hamiltonian systems", *Russ. Math. Surv.*, vol. 32, p. 1, 1977.

[9] A. Bazzani, S. Marmi, and G. Turchetti, "Nekhoroshev estimate for isochronous non resonant symplectic maps", *Cel. Mech.*, vol. 47, p. 333, 1990.

[10] G. Turchetti, "Nekhoroshev stability estimates for symplectic maps and physical applications", in *Proc. of the Winter School*, vol. 47, p. 223, 1990.

[11] P. Belanger, "Topological formulation of beam dynamics: a study of quasiperiodic motion in hamiltonian systems". doi:https://doi.org/10.17181/r1fdr-2hh33

[12] A. Bazzani, G. Servizi, E. Todesco, and G. Turchetti, "A normal form approach to the theory of nonlinear betatronic motion", CERN, Geneva, Rep., 1994. doi:10.5170/CERN-1994-002

[13] J. Laskar, C. Froeschlé, and A. Celletti, "The measure of chaos by the numerical analysis of the fundamental frequencies. Application to the standard mapping", *Physica D: Nonlinear Phenomena*, vol. 56, no. 2, pp. 253–269, May 1992. doi:10.1016/0167-2789(92)90028-L

[14] J. Laskar, "Introduction to Frequency Map Analysis", en, in in *Hamiltonian Systems with Three or More Degrees of Freedom*, ed. by C. Simó, Dordrecht: Springer Netherlands, 1999, pp. 134–150, ISBN: 978-94-011-4673-9, doi:10.1007/978-94-011-4673-9_13,

[15] A. Wolski, "Methods for Analysis of Single-Particle Dynamics", in in *Beam Dynamics in High Energy Particle Accelerators*, Imperial College Press, Apr. 2013, pp. 331–391, ISBN: 978-1-78326-277-9, doi:10.1142/9781783262786_0011,

[16] J. Laskar, "Frequency map analysis and quasiperiodic decompositions", 2003, arXiv: math/0305364 [math.DS], https://arxiv.org/abs/math/0305364,

[17] "Nafflib: NAFF algorithm for frequency analysis", https://github.com/xsuite/nafflib,

[18] "Pytori: Transport of loops and tori in accelerator beam lines", https://github.com/pbelange/pytori,

[19] P. Belanger and G. Sterbini, "Numerical evaluation of the integrals of motion in particle accelerator tracking codes", 2025. doi:10.48550/arXiv.2503.19122

[20] E. Lamb, G. Sterbini, and H. Bartosik, "Luminosity effects due to dependent heavy-tailed beams", in *Proc. IPAC'24*, Nashville, TN, USA, pp. 55–58, Jul. 2024. doi:10.18429/JACoW-IPAC2024-MOPC09

[21] G. Sterbini, H. Bartosik, I. Efthymiopoulos, and S. Kostoglou, "Do transverse bunch tails produce luminosity?", in *Proc. IPAC'25*, Taipei, Taiwan, pp. 314–317, Nov. 2025. doi:10.18429/JACoW-IPAC2025-MOPM017